







## The mechanics of iron tailings from laboratory tests on reconstituted samples collected in post-mortem Dam I in Brumadinho

António Viana da Fonseca<sup>1</sup> , Diana Cordeiro<sup>1</sup> , Fausto Molina-Gómez<sup>1</sup> ,  
Davide Besençon<sup>1,2</sup> , António Fonseca<sup>1</sup> , Cristiana Ferreira<sup>1#</sup> 

Article

### Keywords

Geotechnical laboratory tests  
Iron ore tailings  
Critical state soil mechanics  
Tailings dam failure  
Instability  
Liquefaction

### Abstract

Dam B1 was approximately 85 m high and 700 m long along the crown when it suddenly failed in 25<sup>th</sup> of January, after 41 years of operations and deposition of tailings at the Paraopeba mining complex (Córrego de Feijão), in Minas Gerais, Brazil. More than 250 people died and vast economic, social and environmental damages resulted from the collapse. Given the need to geotechnically characterise the tailings within the dam for a credible computational model of the failure, an extensive sampling and laboratory testing campaign took place. The geotechnical laboratory of the Civil Engineering Department at the Faculty of Engineering of the University of Porto (Portugal) was invited by CIMNE, under a contract with VALE, with MPF agreement, to conduct this program. This paper will present a description of the sampling campaigns in the remaining post-mortem dam/reservoir tailings where the failure instability mechanics developed and the experimental program undertaken to test the tailings in advanced laboratory tests. The results that embrace evaluations of the physical, hydraulic and mechanical properties, deduced from integral samples selectively collected and prepared as described, which allowed to define the geotechnical parameters necessary for the referred analyses are here resumed.

## 1. Introduction

Dam I in the municipality of Brumadinho suddenly failed at 12:28 p.m. local time on January 25<sup>th</sup> of 2019, after more than 40 years of operation and deposition of tailings processed from the natural rocks extracted from the Córrego de Feijão mine of the Paraopeba Complex, in Minas Gerais (MG), Brazil. The recorded images showed that the dam failure was sudden and abrupt, with no apparent signs of distress prior to the failure, developing across approximately 80% of the face of the dam in about 5 seconds. The failed slope material quickly turned into a mudflow. LiDAR post-failure topography indicates that 9.7 Mm<sup>3</sup> of material were lost from the dam, which approximately corresponds to 75% of the pre-failure volume, causing a catastrophic damage downstream and is considered one of the most dramatic tragedies in recent years, in Brazil (Figure 1). As a direct consequence of the failure, many people died and vast economic, social and environmental damages were caused. The failure was the result of flow (static) liquefaction within the materials of the dam (Robertson et al., 2019).

Dam B1 was approximately 85 m high and 700 m long along the crest when it failed. The tailings disposal had stopped about 2.5 years before the failure and no large-scale operations were being performed at the time. The dam's construction history provides insight as to the possible reasons for the failure. The deficient upstream construction and the poor drainage conditions created a dam that was composed of mostly loose, saturated, heavy, and brittle tailings that had high shear stresses within the downstream slope, resulting in a marginally stable dam (i.e., close to failure in undrained conditions). What remained unclear was how the liquefaction process was initiated i.e., what was the event that started shearing in some region of the dam and triggered the liquefaction response. Special attention was given to the operations going on during the last year before the failure, namely the sub horizontal drilling operations to install drains and the perforation of vertical boreholes to install piezometers.

Extensive forensic activities and post-liquefaction studies, including advanced numerical simulations, were carried out to understand the tailings behaviour and response

<sup>#</sup>Corresponding author. E-mail address: cristiana@fe.up.pt

<sup>1</sup>CONSTRUCT-GEO, University of Porto, Faculty of Engineering, Porto, Portugal.

<sup>2</sup>Escuela Superior Politécnica del Litoral, Facultad de Ingeniería en Ciencias de la Tierra, Guayaquil, Ecuador.

Submitted on February 4, 2022; Final Acceptance on March 31, 2022; Discussion open until August 31, 2022.

<https://doi.org/10.28927/SR.2022.001122>



This is an Open Access article distributed under the terms of the Creative Commons Attribution License, which permits unrestricted use, distribution, and reproduction in any medium, provided the original work is properly cited.



**Figure 1.** Google Earth images of the dam: (a) image on 22/7/2018; and (b) image after the collapse (22/12/2019).

mechanics and to objectively determine the probable and/or concurrent causes that led to the failure of this dam. Technical investigations on the causes of Dam I failure were commissioned by both the Authorities (the Federal Public Prosecutor’s Office) and the owner of the mining complex (Vale SA). Three main reports on the technical causes of the failure of Feijão Dam 1 were presented based on the results of those investigations:

- the Expert Panel Technical Report (EPR) by Robertson et al. (2019);
- an independent investigation conducted by CIAEA, whose report is not public;
- the Computational Analysis Report by CIMNE (2021).

Given the need to geotechnically characterise the tailings within the dam for a credible computational model of the failure, an extensive sampling and laboratory testing campaign took place. The Geotechnical Laboratory (LabGEO) of the Civil Engineering Department at the Faculty of Engineering of the University of Porto (Portugal) was invited to conduct the advanced testing program.

This paper describes the experimental program, including the sampling of a large set of undisturbed and reconstituted samples in the post-mortem Tailings Storage Facility (TSF), and the procedures of the laboratory tests. The results obtained from the basic/conventional to the more advanced techniques, using the appropriate methodologies provided the parameters for the construction of constitutive models for numerical simulations. The laboratory procedures included the reconstitution of representative specimens in diverse state conditions and the execution of a wide variety of both conventional and advanced laboratory tests in these specimens. The materials were collected in three different locations near the failure zone. The number of different soils was carefully selected, considering the previous discretisation of limited clusters inside the deposited masses based on in situ tests –performed prior to the failure. The tests result embraced evaluations of the physical, hydraulic and mechanical properties, allowing the definition of fundamental

parameters for the inputs of appropriate constitutive models based in Critical State Soil Mechanics (CSSM) and capable of reproducing a wide range of soil behaviour, from ductile to very brittle, especially the undrained softening underlying the flow liquefaction phenomenon.

## 2. Site description and material selection

### 2.1 Considerations about the objectives

With a view to adopting physical, hydraulic and geomechanical parameters representative of the materials involved in the behaviour of this complex soil system, it was necessary to reassess the available results. The models that were adopted for the numerical analysis required the execution of tests of various complexities, from the most elementary (but no less important) to the more advanced, capable of defining the model parameters that would cover the essentials of the mechanical behaviour in conventional soils, but also in liquefiable soils. However, the geotechnical information obtained from previous studies presented significant gaps that were directly relevant to the numerical model under preparation. In particular, there were reasonable doubts about how representative of the dam materials involved in the failure were those selected for testing by the EPR. There were very few laboratory data with reliable measurements of undrained strength in conditions (initial state, consolidation history) similar to those prevailing in the field and there were no systematic data on possible strain rate effects on strength, which was unfortunate considering that viscous creep had been postulated as a possible triggering factor by the EPR (CIMNE, 2021). Therefore, it was considered necessary to obtain new samples from the remaining dam material and to extensively test them in the laboratory.

The nature of the tailings deposited in this TSF had to be dealt with great care. The representativeness of the samples to be retrieved from this huge volume of deposited tailings was carried out in light of strict analyses of historical registered data of the 50 years rising this TSF. More importantly, a



**Figure 2.** Examples of localised layer variability: (a) layering visible in the field; (b) micro layering, visible on an undisturbed sample from Site 1 (12/19/2019) at LabGEO.

representative number of recently performed in situ tests data; that is, static cone penetration tests with measurement of pore pressures (CPTu) and shear wave velocities ( $V_s$ ) by seismic flat dilatometer devices (SDMT). The CPTu and  $V_s$  profiles were analysed before the decision to program the campaigns to obtain new samples in the remains of the dam revealed an expected high variability/heterogeneity in depth as well as in plan. It was clear that the materials involved in the modelling process should be associated to the deposition phases along the years (when distinct mining fronts and injection/spigotting explain the variability). The interlayering was clear in the intact samples directly obtained in the remaining intact blocks, as observed in the trenches created for such purpose. A very thin layer interstratification and anisotropy at lab scale were also observed (see Figure 2).

Testing these intact/undisturbed samples is important to identify how the results fit into the general framework of each type of material selected to constitute the numerical modelling. It is very difficult to pass from the specificities of these undisturbed stratified (“individual” material distribution and facies, with specific behaviour) to an extrapolation for a unified model of each of the constituents. Therefore, a meticulous identification of burses of more homogeneous masses was carried out and the integral masses (mainly referred to convergent colours with distinctive values specific gravity) were assembled in bags and taken to the laboratory.

This representativeness was naturally highly limited by the condition of the depleted basin and the almost complete disappearance of the dam’s lifting dykes built upstream. However, as will be explained in what follows, areas were sought that contained undisturbed material and different typologies that emerged from the analysis of the public elements available from reports by previous expert panels.



**Figure 3.** Location of the three sampling sites on B1 dam, after failure.

## 2.2 Sampling campaigns

The campaigns to collect representative samples of these tailings were carried out in three phases. The first campaign (S1) was carried out on 19<sup>th</sup> December 2019, the second (S2) on 26<sup>th</sup> December 2019, and the third (S3-L1 and S3-L4) on the following 12<sup>th</sup> March 2020. Figure 3 identifies the location and date of the three campaigns in the post-mortem condition of the dam.

After a precise visual identification of the exposed area of the remains of the dam, the first campaign was led to the integral masses (still standing or moved down but preserved) deep in the tailings, to the bottom of the basin of the destroyed dam and heading towards the right margin of the dam. The two other campaigns were conducted in view of the need for additional types of soils and samples for the programmed laboratory tests. These site investigation works were coordinated by the first author, in collaboration with

Professor António Mendonça from the Federal University of Minas Gerais (UFMG) and the local technical support of VALE.

Two materials were identified as prevailing in Site 1 with quite distinct visual properties, namely a red fine tailing material and a dark (black) granular one. These materials clearly differed on some faces from the large masses that had failed –probably due to the relief of the internal part of the drainage basin– along the exposed slide surfaces in a progressive process. As these were shallow areas closer to the basin margins, they did not collapse, but rather slid along these surfaces at the limit of frictional resistance. So, in the very first campaign, it was realised that it would be possible to find “undisturbed” tailings, that is, not collapsed and with the original fabric and inter-particle structure, allowing the execution of several tests in the laboratory if they were directly sampled with thin-walled blocks and tubes, as illustrated in Figure 2a).

The second visit to the dam took place on December 26<sup>th</sup>, 2019, but it was not possible to access areas within the

volume of the rupture due to the heavy rainfalls at the end of that year, and it was necessary to move to more secure areas behind the crest. On Site 2, located inside the tailing’s reservoir, a brown very fine material was collected for its abundance. Small clusters of red/brownish material were also gathered. A large number of intact/undisturbed samples was also retrieved from this location.

Later on, a third campaign (Site 3) was carried out, and two locations were accessible (these were named S3-L1 and S3-L4). The Local 1 was situated in the upper part of the previous Site 1, in slipped masses difficult to access and where black horizons were dominant, while Local 4 was close to the abutment where the soils from the EPR campaign were collected (see Figure 4). Bags with remoulded but integral samples were collected from each site avoiding segregation and respecting the grain size distribution of the sampled volume of homogenised soil. Intact/undisturbed tailings were also block sampled in these locations.

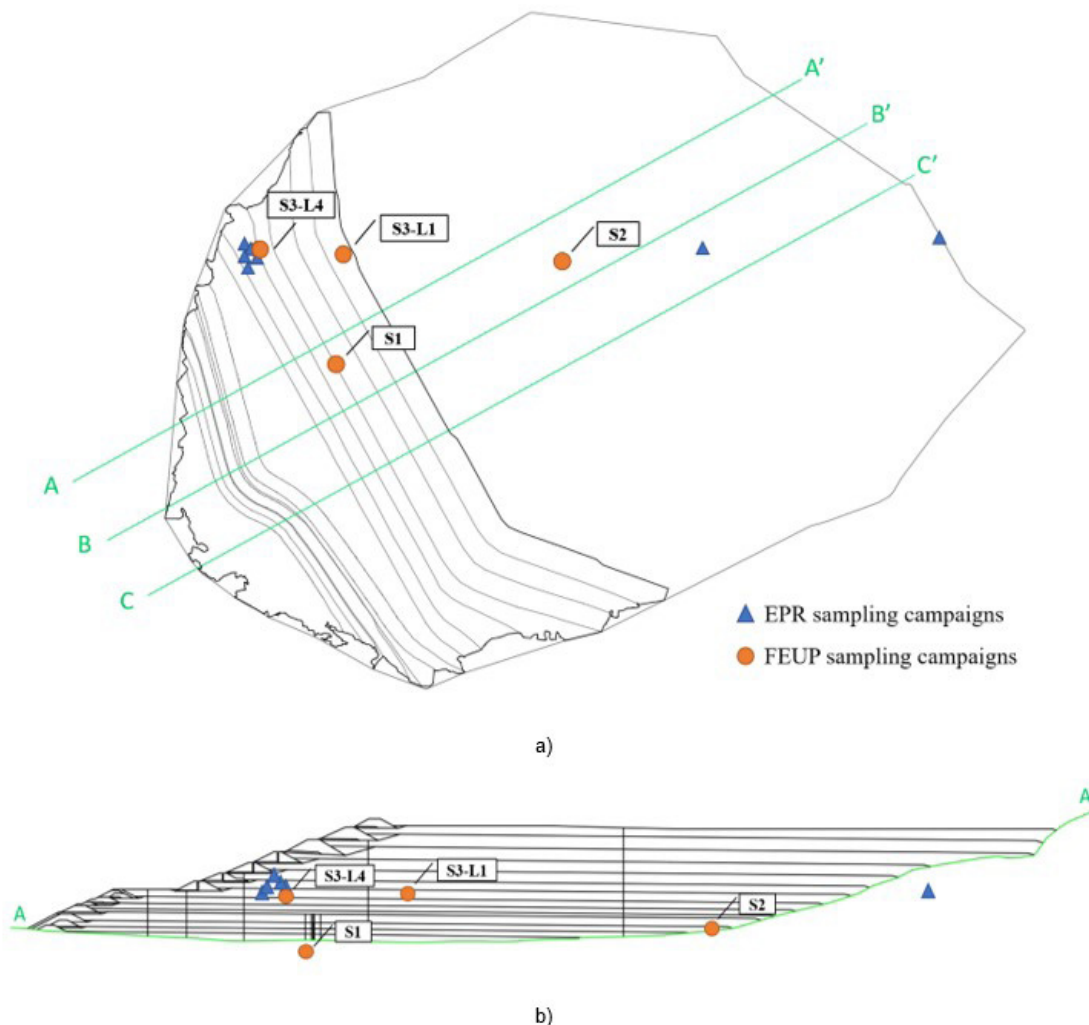


**Figure 4.** Location of the experimental sites from the different sampling campaigns – Projected position: (a) plan view of the dam; (b) alongside the dam section.

EPR and FEUP sampling locations are projected in Figure 4 on the plan view of the dam and alongside the dam section reference axis A-A'. Most samples from the EPR were clustered at a single location close to the remains of the left abutment of the dam (taken from levels corresponding to intermediate dam filling stages), while other two sites were several hundred meters behind the last crest of the dam, with the intention of recovering slimes. The initial failure surface was very far away from these sampling locations.

FEUP experimental sites are deeper and correspond to older tailings than those obtained in the EPR campaign, except for Site 2, located 200 m behind the final crest of the dam, which was chosen with the intention of recovering slimes. Notwithstanding, FEUP sampling sites are likely closer to the location of the initial failure surface.

### 2.3 Material selection

Geotechnical characterization of the tailings that constituted the dam was deemed essential to obtain a credible computational model of the failure, but from a practical and effective point of view, a discretisation of limited clusters/blocks inside the deposited masses was pursued. This is well described in the referred CIMNE panel report. In order to simplify the numerical analyses, two modelling decision were investigated: how many materials can fairly represent the complex distribution of tailings through the dam (heterogeneously distributed and strongly interlayered); and which of the collected materials are compatible with the dominant soil behaviour types present along the dam (coarse to fine granular tailings, silty sands, mostly silts and even slimes).

This subject was initially addressed by analysing the proficuous data from several CPTu testing campaigns during the period from 2005 and 2018. The soil behaviour type index  $I_{c_{RW}} = 2.60$  proposed by Robertson & Wride (1998) is normally used to separate fine from coarse material. This threshold value has been observed to separate correctly mostly granular and mostly cohesive soils in natural deposits; however, it is unclear if this value is also the best for tailings.

Aided by advanced numerical simulations, CIMNE established a different threshold for  $I_{c_{RW}}$  based on the drained and undrained response to CPTu tests, to a higher value of 2.85, optimising the fine and coarse behaviour type horizons. Soils that respond in a drained manner to CPTu penetration would be very permeable. Therefore, permeability was the key property to differentiate fine from coarse soils, and, in this case, was also correlated with important critical state properties. The undrained response to a CPTu was quantified by the normalised excess pore pressure index  $B_q$ .

The coarse ( $I_{c_{RW}} < 2.85$ ) and fine ( $I_{c_{RW}} \geq 2.85$ ) fractions of tailings were not homogeneously distributed in the dam body. CPTu results showed that stage changes (different deposition phases) were often coincident with significant changes in mechanical response. To simplify the spatial

distribution of tailings within the dam, blocks were created in the diverse analysed sections by CIMNE. These blocks correspond to a specific section, raising and alignment of the dam and have some allocated data from the corresponding CPTu tests. For practical reasons, only a limited number of material types can be used in the numerical simulation. Thus, CIMNE decided to use three different types of tailings to assign material properties to the different blocks in the model.

Three materials were idealised, covering all material distribution: Fine tailings (when the CPTu indicated a proportion of Fines Content, FC, equal or above 50%); Coarse tailings (when the CPTu indicated a proportion of FC equal or below 10%) and Mixture tailings (for CPTu FC between 10 and 50%). The objectiveness in the sampling campaigns was crucial to retrieve best "material models" in soil behaviour types.

FEUP investigated all remoulded/integral and intact/undisturbed samples obtained in the different sampling campaigns. From the physical properties (mainly particle size distribution, PSD and specific gravity,  $G_s$ ) and the coloration of the materials found, it was selected a set of three ideal materials to be representative of different tailing materials within the dam identified in the CPTu analyses. The typological classes of soils were named as Type 1 for red fine tailing material collected on Site 1; Type 2 for the brown very fine material collected on Site 2; and Type 3 for the black granular material collected on Site 1.

The undisturbed samples were not selected to define the numerical modelling, as it is very difficult to overcome the specificities of these undisturbed stratified materials to an extrapolation for a unified model of each of the constituents. They will however be addressed in future works. The red/brownish material collected from Site 2 was not considered representative of the tailings reservoir, as it showed a combination of physical characteristics of the soils under evaluation. The samples retrieved from Site 3-Local 4 were also not considered in the numerical modelling as they were too close to the embankment berm and further to the location of the initial failure surface. Nonetheless, after analysing the integral samples collected from Site 3-Local 1, the black coarser tailing was considered an ideal material to be representative of different tailing materials within the dam, given its brittleness and proximity to the initial failure surface location. This material, named Type 4, was not included in the dam's modelling, as it was still being tested and its mechanical characterisation will be presented in an independent paper.

The ideal reconstituted materials tested in this program show similarities in grain size distribution, in comparison with those tested by EPR. However, these materials are more distinctive than those of the EPR, with respect to the more fundamental physical properties (such as the specific gravity,  $G_s$  and the shape of the particle size distribution, expressed by the coefficient of uniformity,  $C_u$ ), for which they almost cover the full range present on the tailing samples.

This division into three typological groups would be later confirmed by the results obtained in laboratory tests for the determination of hydraulic conductivity (permeability), volumetric compressibility in confined conditions (either in isotropic loading or in oedometric loading –unidirectional) and shear strength resistance, in diversified conditions. This extensive and varied testing program had to be developed in a work of such complexity, since different drainage conditions (total drained – or inhibited – not drained) and loading paths must be considered.

### 3. Geotechnical characterisation of the tailing materials

#### 3.1 Experimental methodology

At an early stage of this process, after visual inspection of the collected soil samples, it became clear that, in order to achieve a broad and comprehensive geotechnical characterisation of the tailing soils of the case study dam, it was necessary to consider different soil types to be tested and analysed in parallel. As such, the typological classes of soils considered representative of the tailings stored in the dam were defined, based on the characteristics of the samples collected during the sampling campaigns previously described, having been selected and identified the following three types of tailings:

- Type 1 – Fine reddish, low-ferrous tailings;
- Type 2 – Fine brownish, moderately ferrous tailings;
- Type 3 – Coarse-grained black iron-rich tailings.

The final selection of these three types of tailings materials was supported by two physical criteria, namely the particle size distribution (PSD) and the specific gravity of the solid particles ( $G_s$ ). Fine and coarse designation associated with significant distinct permeability values as expressed before. These two criteria were adopted, since it is recognised that soil grading controls the behaviour of the soil, while the different values of the  $G_s$  can be associated with the iron content of each tailing.

The experimental program was designed to include laboratory tests that objectively determine the necessary parameters for the calibration of the constitutive models required to perform specialised computational analyses. Therefore, an extensive series of tests was carried out for a general geotechnical characterisation, namely physical, hydraulic and geomechanical parameters, in terms of compressibility and shear strength. The experimental program comprised grain size distribution, specific gravity of solid particles, hydraulic conductivity (permeability in different isotropic stress levels), volumetric compressibility in confined conditions (in isotropic and unidirectional oedometric loading) and strength characterisation in diverse triaxial testing conditions. This experimental plan was discussed with Professors Antonio Gens and Marcos Arroyo, the main authors of the CIMNE report.

Special attention was given to the ultimate strength at constant volume, which is fundamentally mobilised under ‘stable’ behaviour (i.e., critical state condition). For this purpose, tests involving different stress-paths and drainage conditions, necessarily associated with the complex geotechnical structure of the Dam I, were considered. The failure resulting in a flow slide was the result of flow liquefaction within the tailings in the dam. Since only contractive materials have the possibility of undergoing liquefaction, particular emphasis was given on undrained behaviour of very loose samples. The EPR also concluded that the sudden strength loss and resulting failure of the marginally stable dam was due to a critical combination of ongoing internal strains due to creep, and a strength reduction due to loss of suction in the unsaturated zone caused by the cumulative rainfall. For this purpose, a series of triaxial tests were explicitly designed to investigate strain rate effects on undrained strength of tailings.

#### 3.2 Physical characterisation

The particle size distribution analyses and specific gravity were performed according to ISO 17892-4 (ISO, 2016) and ISO 17892-3 (ISO, 2015) standards, respectively, like the corresponding ASTM standards. Figure 5 illustrates the results of the particle size distribution curves of the three types of tailings identified, together with a shaded area corresponding to the reported grading curves of the collected tailings soil samples, as published in the EPR (Robertson et al., 2019).

Soil type 1 corresponds to fine reddish, low-ferrous tailings, with a specific gravity of 3.94. Soil type 2 refers to a fine brownish, moderately ferrous tailings, with specific gravity is equal to 4.55. Soil type 3 is a coarse-grained

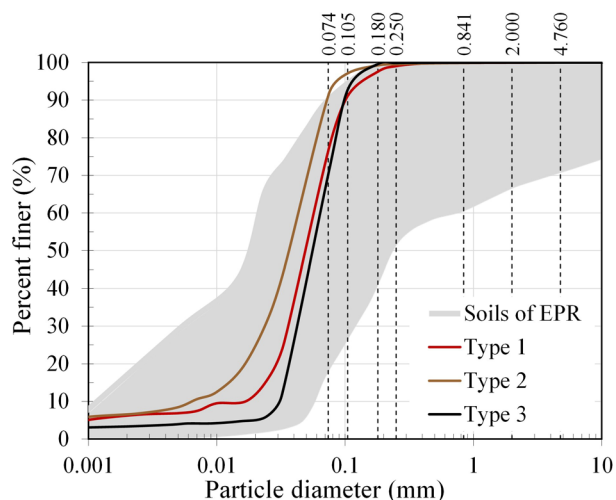


**Figure 5.** Grading curves of the three types of tailings. Comparison with other soils from Brumadinho dam, according to the Expert Panel Report (EPR) (Robertson et al., 2019).

black iron-rich tailing, with the highest specific gravity of 5.00. The distinct particle densities are related to the initial stages of the tailing depositions, when the process of extracting iron ore from the rocks coming from the mine was less efficient. The percentage of iron is much higher in the dark tailings, produced in the first rising phases of the dam, than in the red, corresponding to more recent operations.

### 3.3 Compressibility and consolidation characterisation

#### 3.3.1 Oedometric compressibility

Several oedometer consolidation tests were performed to assess the compressibility of the three types of tailings identified in the previous section. The testing process followed the international standard ISO 17892-5 (ISO, 2017). These tests were carried out on remoulded samples using the moist tamping technique, ensuring a loose soil state condition. In-situ void ratios were derived from the analysis of several CPTu tests carried out at different locations and undisturbed block samples tested in the laboratory in this study. Comparisons, prior to the dam failure, between initial void ratios of samples collected during the deposition stages presented systematically dilatant behaviour when tested in the laboratory. These contradict the high values of state parameters derived from CPT and CPTU tests, pointing to contractive behaviour. Knowing that critical state locus is reached independently of the initial void ratio and that it is more clearly reached in triaxial tests from the loosest possible state conditions (Viana da Fonseca et al., 2021), the preparation of the specimens was done with the utmost care to obtain higher values than those referred above determined after the failure for this study. After preparing the samples, these were placed in the oedometer cells and submerged in distilled water for a minimum period of 12 hours, to ensure nearly full saturation of the soil. Subsequently, the samples were subjected to a series of loading and unloading stages to establish the compressibility parameters of the three types of tailings, as illustrated in Figure 6.

Table 1 summarises the compressibility parameters obtained on the oedometer tests for the three types of tailings. It can be observed that the three types of tailings exhibit different compressibility parameters: compressibility index ( $C_c$ ), recompressibility index ( $C_r$ , obtained from the unload-reload cycles of moderate amplitude), expansion index from the final unload at near zero stress ( $C_s$ ) and other ratios,

namely  $C_c/C_r$ . These differences are demonstrative of distinct geomechanical behaviour according to the type of tailing previously defined. Based on these diverse compressibility characteristics, the selection of the three types of tailings to be characterised in further detail was validated, which will be carried out using advanced techniques, as described in the following sections.

In view of these oedometer test results, it was observed that the three types of tailings exhibited a slope change on the compressibility curve for effective vertical stresses ( $\sigma'_v$ ) above 3200 kPa. This finding evidences the evolutive nature of these soils, caused mainly by particle breakage (or crushing) or by changes in the shape of particles at higher stresses. On the other hand, no transitional behaviour was observed in these materials, since tests performed at different initial void ratios converged to the same 1D compressibility line (results not shown here, further details in Annex 1 of the CIMNE report).

#### 3.3.2 Isotropic compressibility

A series of isotropic consolidation tests were carried out in triaxial cells as complement to the oedometer consolidation tests, in order to characterise the soil stiffness parameters established in the critical state theory. These tests were performed on remoulded loose specimens using the moist tamping technique. The test procedure included the application

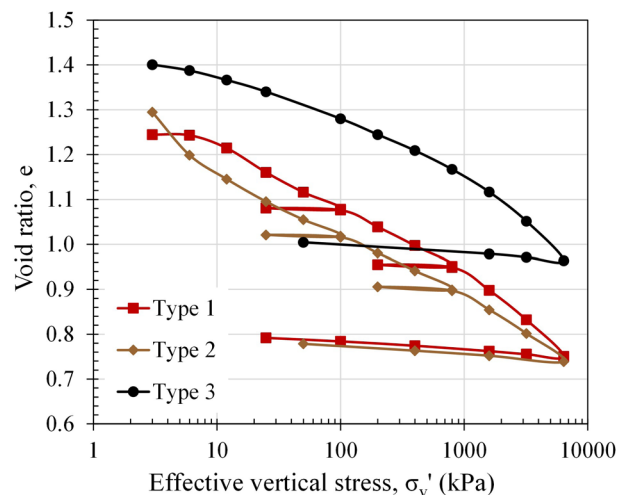


**Figure 6.** Oedometric compressibility curves for the three different tailings.

**Table 1.** Oedometer compressibility parameters for the three tailings soil types.

ID	Soil type	$e_0$ (-)	$C_c$ (-)	$C_r$ (-)	$C_c/C_r$ (-)	$C_s$ (-)
ED_T1	Type 1	1.24	0.2196	0.0097	22.64	0.0181
ED_T2	Type 2	1.30	0.1589	0.0143	11.11	0.0175
ED_T3	Type 3	1.40	0.1925	0.0267	7.21	0.0254

ID: Identification.

of several consolidation stages, with measurement of the volumetric change over time. Since the triaxial cells used for these tests were equipped with bender elements (BE), seismic shear wave velocities,  $V_s$ , were measured to estimate the variation of the small-strain stiffness at each consolidation stage, according to the methodology proposed by Viana da Fonseca et al. (2009) and Ferreira et al. (2021). In addition, seismic compressional wave velocities,  $V_p$ , were measured to assess the saturation conditions, complementing the verification by Skempton's B parameter, as recommended by Viana da Fonseca et al. (2021). Figure 7 shows the isotropic compressibility curves in the  $e - \log p'$  plane, for the three different tailings.

Table 2 includes the isotropic compressibility parameters obtained from the isotropic consolidation tests with seismic wave measurement, where it is confirmed that the three types of tailings present distinct behaviour, as previously verified in the oedometer tests.

### 3.4 Small-strain stiffness

Small-strain stiffness was measured by means of bender elements during triaxial testing of the different types of tailings. These piezoelectric transducers, which send and receive seismic waves, allow the measurement of P and S-wave velocities at any stress conditions during the triaxial test. The required equipment consists of a function generator (TTi TG1010), an oscilloscope (Tektronix TDS 220) and a

**Table 2.** Isotropic compressibility parameters for the three tailings soil types.

Material	N (-)	$\lambda_c$ (-)	$\kappa$ (-)
Type 1	1.1944	0.049	0.006
Type 2	1.0873	0.046	0.003
Type 3	1.3129	0.028	0.003

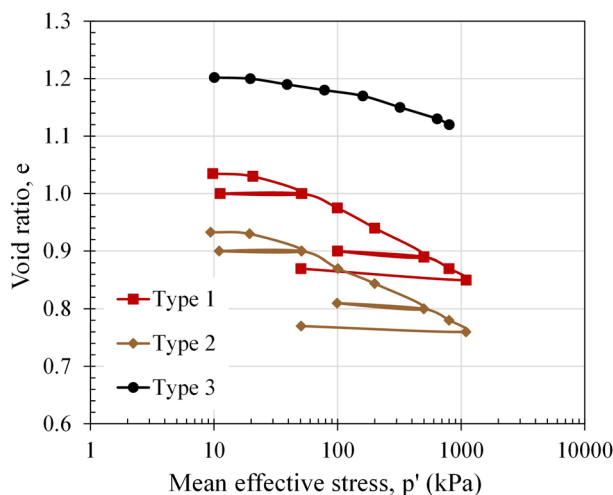


**Figure 7.** Isotropic compressibility curves for the three types of tailings.

computer for signal acquisition. In these tests, a series of single sinusoidal pulses at different input frequencies was used to excite the transmitter BE, to minimise the uncertainty and subjectivity associated with signal interpretation (Viana da Fonseca et al., 2009). For S-wave measurement, input frequencies ranged from 1 to 10 kHz were used, from which the results in Figure 8 were obtained for the three different tailings.

These results indicate a higher stress-dependency for Type 1, evidenced by the higher stress exponent, which is typically observed in soils with a weaker fabric or inherent structure. Globally, it can be observed that the denser soils exhibit a lower stress-dependency. Further analyses of this behaviour are currently being performed as complementary studies.

P-waves were also measured, using frequencies between 25 to 150 kHz, mainly to assess the saturation conditions of the tested specimens. As established in the wave propagation theory, if the value of the compression wave velocity ( $V_p$ ) is greater than 1482 m/s, the soil is saturated (Santamarina et al., 2001).

### 3.5 Hydraulic conductivity/permeability

The hydraulic conductivity or permeability of the three types of tailings was measured by direct constant head permeability tests measured in triaxial cells. The test procedure included soil saturation, by increasing the backpressure up to 300 kPa, while maintaining the same effective confinement of 10 kPa, followed by the flow of deaired water by applying a constant head of about 5 kPa between the ends of the specimen (e.g., 302.5 kPa at the bottom and 297.5 kPa at the top). The determination of the coefficient of hydraulic conductivity ( $k$ ) of the different soils was carried out at several loading stages and void ratios. Figure 9 shows the

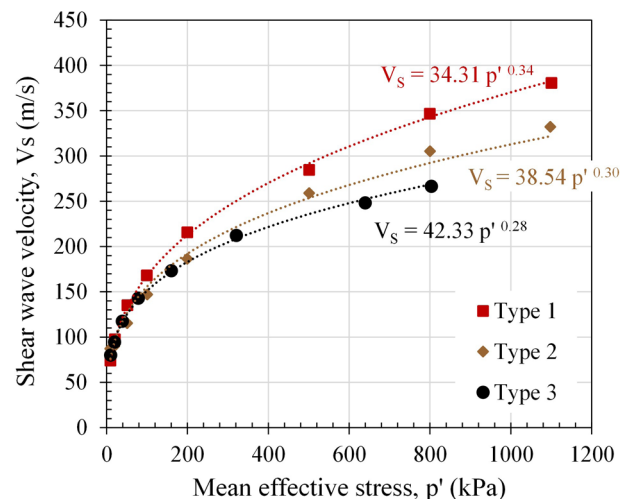


**Figure 8.** Evolution of shear wave velocities as a function of mean effective stress for the three types of tailings.



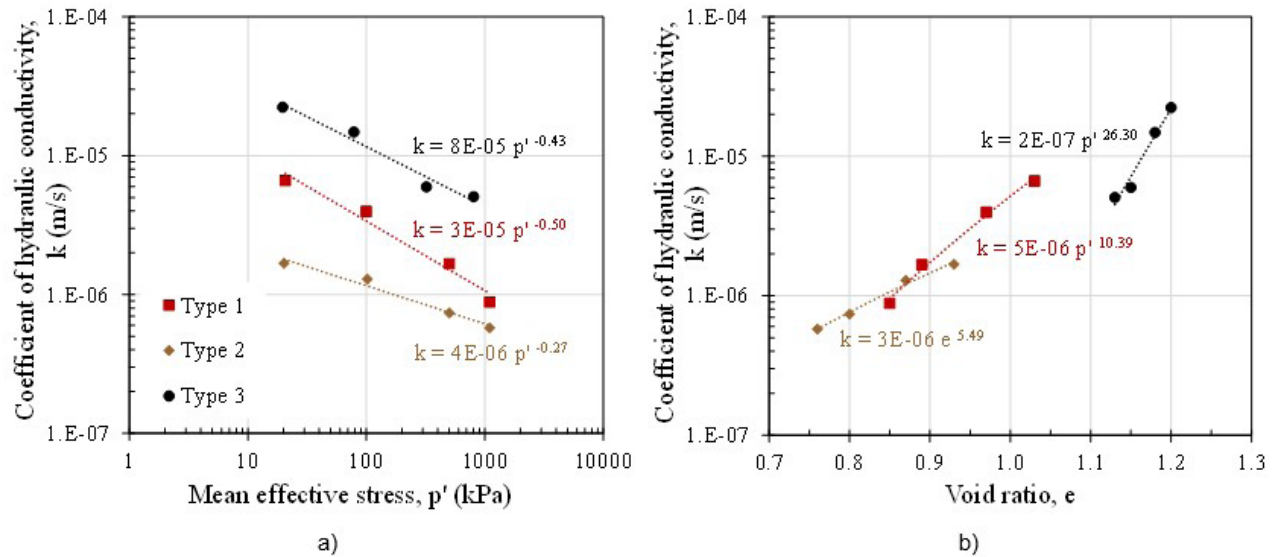


**Figure 9.** Variation of the coefficient of hydraulic conductivity for the three types as a function of: (a) effective stress conditions; (b) void ratio.

coefficient of hydraulic conductivity curves for the three tailings as a function of the effective stresses and void ratio conditions. The void ratios presented in this figure correspond to the estimated values at each loading consolidation stage, in which permeability was measured.

From Figure 9, it can be observed that the three types of tailings have different permeability characteristics, which is a clear indication of distinct soil behaviour. Since the order of magnitude of permeability is correlated with the particle size distribution of the materials, there is an evident correspondence between these parameters and the grading properties of each type of tailings. Based on the differences in permeability coefficients, the selection of the types of tailings to be characterised is validated.

## 4. Critical state characterisation

### 4.1 Specific equipment and procedures

Critical State Soil Mechanics (CSSM) has been increasingly applied to describe the behaviour of these granular mine tailings materials, with clear advantages for its modelling, namely for the stability analyses. The critical state line (CSL) of any soil is independent of its initial stress state and its void ratio, thus representing an ‘ultimate and stable state’ and can be estimated from laboratory triaxial tests. The results allow obtaining the shear-confinement-volume state, represented by three-dimensional invariants in the  $e-p'-q$  plane (void ratio, mean and deviatoric effective stresses). The definition of critical state lines (CSL) for each type of tailings was carried out by performing a set of triaxial tests in drained and undrained conditions. Table 3 summarises the adopted testing program for the CSL characterisation, for the three types of tailings.

The critical state parameters of the iron tailing soils were obtained by following the recommended testing procedures proposed by Viana da Fonseca et al. (2021). Hence, triaxial apparatuses were configured to assess the soil behaviour at large deformations by including lubricated end platens and an embedded connection piston into the top cap. The lubricated end platens allowed uniform radial strains and holding the cylindrical shape of the specimen at large axial strain levels (Molina-Gómez & Viana da Fonseca, 2021); while the embedded connection piston allows significantly reduced tilting of the top cap during all phases of triaxial testing (Reid et al., 2021).

All specimens were prepared using the moist tamping technique simultaneously with the under-compaction method (Ladd, 1978). This preparation procedure was selected due to their reliability, reproducibility and capability to achieve a full range of densities (Jefferies & Been, 2016). Although moist tamping with under-compaction method does not represent well the in-situ deposition of tailings, for critical state characterisation this is not an issue, since the critical state parameters are independent of the initial soil fabric (Smith et al., 2019; Molina-Gómez & Viana da Fonseca, 2021; Reid et al., 2021). The preparation comprised the compaction of six layers at a specific water content, which varied from 5% to 10% according to the soil type and a percent of undercompaction ( $U_n$ ) of 2%. Such procedure ensured the testing of uniform loose samples of 70 mm diameter and 140 mm height –suitable to well-define the critical state locus (CSL) of the studied soils. All specimens were tested in fully saturated conditions. The saturation procedure covered the following phases (Viana da Fonseca et al., 2021): (i) flushing of with 1.5 litres of  $CO_2$  from the bottom drainage line, forcing the air to circulate upwards; (ii) the flushing of 800 ml of de-aired water under a positive effective confining pressure

**Table 3.** Summary of CSL testing program for the three tailings soil types.

Type	Soil		Preparation State	Test Type	Consolidation
	Condition				$p'$ (kPa)
Type 1	Original		Loose	CID	50, 200, 400
			Dense	CID	100, 200
	Evolved		Loose	CID	200, 500, 800
			Dense	CIU	400, 800 (x2)
Type 2	Original		Loose	CID	100, 200, 400
			Dense	CID	100, 200, 400
	Evolved		Loose	CID	50, 100, 400, 800
			Dense	CIU	400
Type 3	Original		Loose	CID	20, 200, 800
			Dense	CID	200
	Evolved		Loose	CID	30, 100, 200, 400, 800
			Dense	CIU	600, 800, 1200
			Dense	CID	100 (x3), 200

Legend: CID – isotropic consolidated drained tests; CIU – isotropic consolidated undrained tests.

(e.g., cell pressure 20 kPa, bottom back-pressure 10 kPa and the top at atmospheric pressure); and (iii) the application of backpressure increments at a constant effective stress of 10 kPa until reach 300 kPa. The full saturation condition was validated by measuring Skempton's B-value. The specimens were only considered fully saturated for B-values higher than 0.97. Overall, B-values of about 0.98 were achieved. After saturation, the samples were isotropically consolidated at different mean effective stresses. For CSL definition, soil specimens were sheared under drained and undrained conditions at 0.025 mm/min. Such rate is compatible to ensure the drainage and pore pressure build-up of cohesionless soils.

To ensure the accuracy of the results, data have been corrected for membrane restraint using the method indicated in the standard procedure ISO 17892-9 (ISO, 2018). On the other hand, the estimation of the final void ratio of soil specimens was carried out by measuring the water content after testing. To obtain reliable measurements of the final water content and then the void ratio after triaxial testing, the end-of-test soil freezing (EOTSF) technique was adopted (Soares & Viana da Fonseca, 2016). A database containing the results of this critical state characterisation has been made available in the form of Supplementary data to this paper.

#### 4.2 CSL results

The results of all drained and undrained loose triaxial tests were analysed and those considered to have reached the critical state were used to define the critical state parameters of the different types of tailings. A slight deviation from linearity was observed at low mean effective stresses (mostly in the coarser materials below 100 kPa); those results were not considered for the definition of the CSL. In turn, for finer materials, a close approximation to linearity was noted, for the full range of stresses representative of the field conditions, used in this study. Figure 10 presents the stress

paths on the  $q - p'$  and  $e - \log p'$  invariant plane derived from triaxial test results.

From Figure 10a, c and e, it can be observed that all endpoints define a unique critical state line (CSL) in the  $q - p'$  plane, which is clearly represented by a straight line passing through the origin. The CSL projections define a strength parameter  $M_c$  equal to 1.42, 1.40 and 1.36 for the type 1, 2 and 3, respectively; and the friction angle of shearing resistance at the critical state ( $\phi'_{cs}$ ) varies from 34° to 35°. Figure 10b, d and f shows the best-fit CSL in the  $e - \log p'$  plane. In this study, the straight-linear approach ( $e_{cs} = \Gamma - \lambda_e \ln p'$ ) was considered the best-fit to describe the behaviour of the different types of tailings. Although Type 3 data exhibits a non-linear critical state locus in the  $e - \log p'$  plane, the stresses and relative density states of the curve part of CSL were considered irrelevant in practical engineering applications. The critical state parameters  $M_c$ ,  $\lambda_e$  and  $\Gamma$  deducted for the different tailings are very well aligned with data for other tailings in reference databases (e.g., Smith et al., 2019).

#### 4.3 Stress-dilatancy behaviour

Dense samples were avoided to define the CSL, as they may not reach the ultimate state, mainly due to the non-uniform sample densities and strains that develop if shear localisation occurs during testing. However, in plasticity-based constitutive models, the dilatancy parameters must be defined. Soil dilatancy only considers the plastic volumetric strains because the elastic volumetric strains are very small and, thus, negligible. Therefore stress-dilatancy of dense samples in drained shear is well established as a fundamental aspect of soil behaviour (Been & Jefferies, 2011).

For this purpose, a set of dense samples were tested in drained conditions for each type of tailings. The equipment and procedures used were the same as previously described, except for the preparation method, as

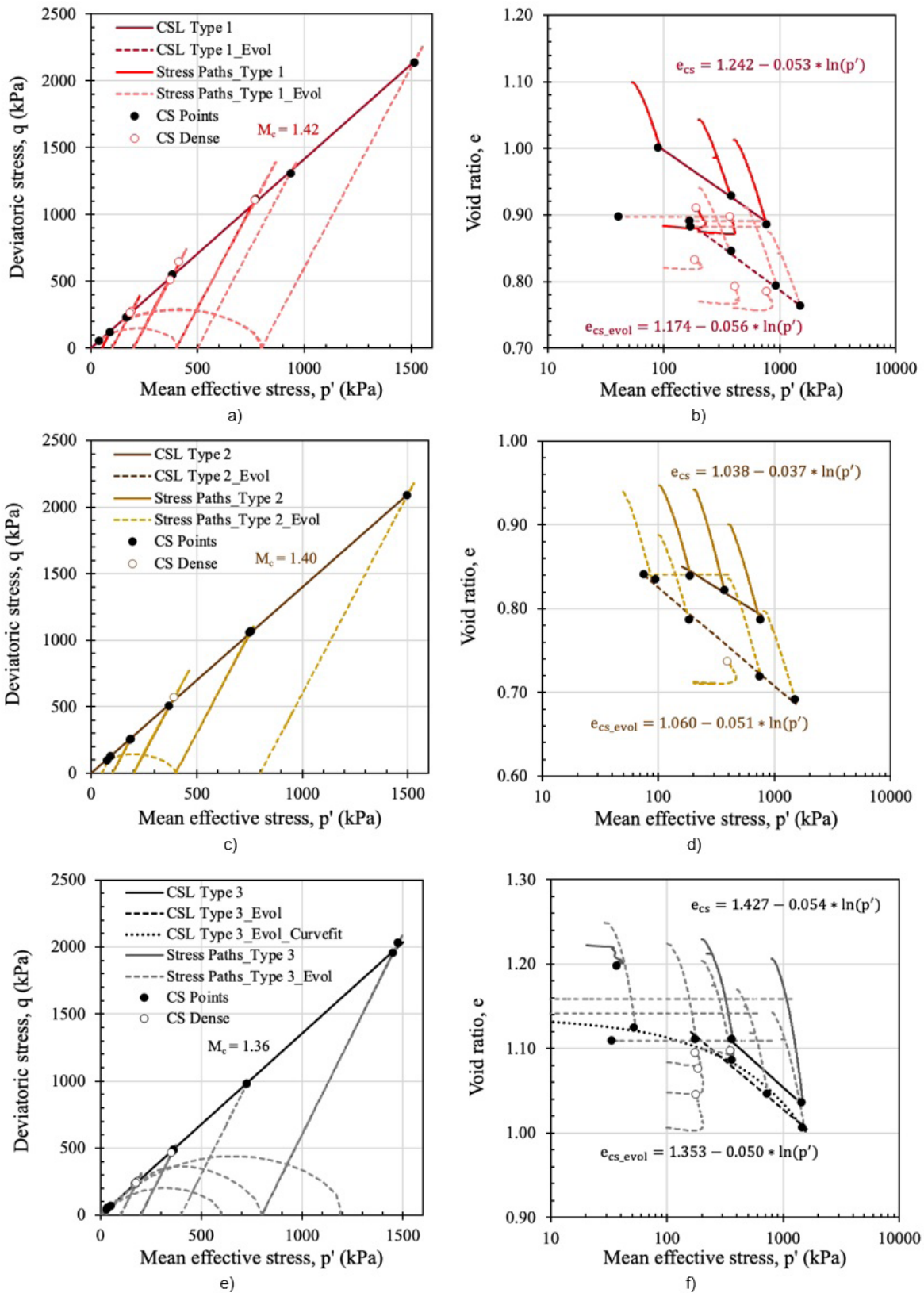


**Figure 10.** Critical state characteristics: (a) results in  $p'$ - $q$  plane of soil Type 1; (b) results in  $e$ - $\log p'$  plane of soil Type 1; (c) results in  $p'$ - $q$  plane of soil Type 2; (d) results in  $e$ - $\log p'$  plane of soil Type 2; (e) results in  $p'$ - $q$  plane of soil Type 3; (f) results in  $e$ - $\log p'$  plane of soil Type 3.

the samples were statically compacted in a loading frame. The stress-state paths derived from the dense triaxial tests are also represented in Figure 11. Table 4 presents the peak values of deviatoric and mean effective stresses with its corresponding void ratio.

## 5. Evidences of soil evolution

### 5.1 Mechanical behaviour evolution

During this experimental program, it became apparent that the behaviour of the three types of tailings evolved, in terms of the CSL positioning in the  $e - \log p'$  plane; that is, in terms of compressibility in shear loading. This evolutive behaviour was first observed after high pressure tests (at mean effective stresses above 800 kPa) and, also, after tests on dense samples (statically compacted at very low

void ratios) and can be attributed to two main factors that affect soil particles, namely the evolution of soil grading and of particle morphology (shape and surface roughness). This evolutive behaviour has been previously reported by Bedin et al. (2012) in gold ore tailings.

During consolidation or shear phases, the material may evolve due to particle breakage or crushing. These processes act as a grinder, increasing the fines content and inducing changes in the shape of the particles. The increment of fines content causes additional compressibility and shifts down the CSL position in the  $e - \log p'$  plane, while changes of particle shape adjust the critical state parameters  $M_c$ ,  $\lambda_e$  and  $\Gamma$ . Such effects generate uncertainties in the CSL position.

The evolution in the behaviour of the three types of tailings was only identified in the  $e - \log p'$  plane, thus, only affecting  $\lambda_e$  and  $\Gamma$ , not  $M_c$  (see Table 5). Therefore, two CSL were defined for each type of tailings, one corresponding to

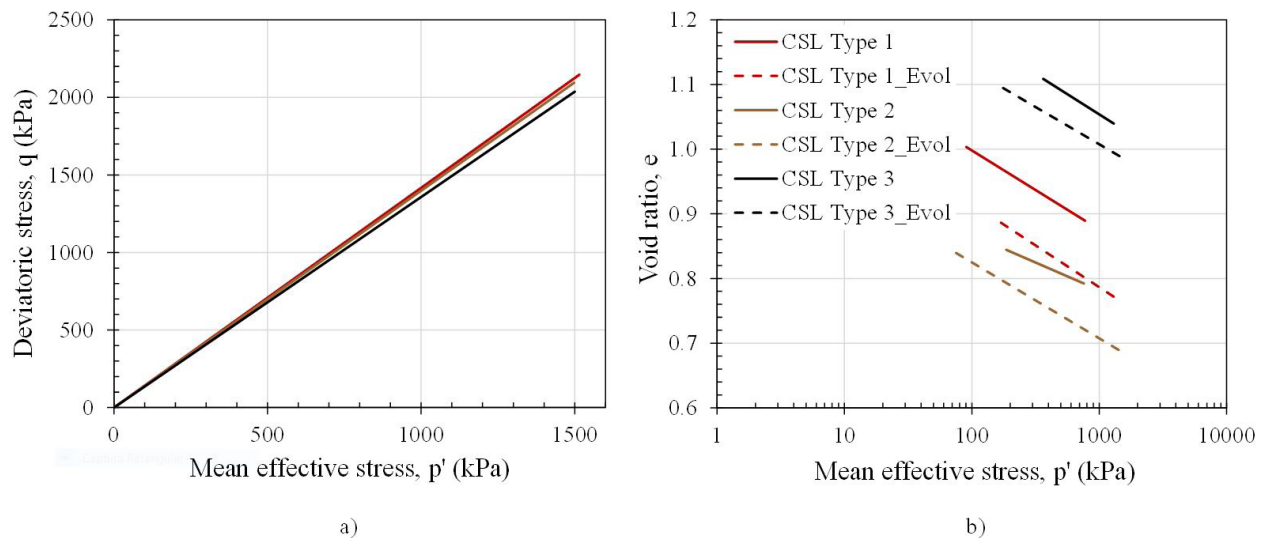


**Figure 11.** CSL of the three types of tailings in natural and evolved conditions in the: (a)  $q - p'$  plot; and (b)  $e - \ln p'$  plane.

**Table 4.** Peak values during shearing for the dense tests.

Soil			Peak Values		
Type	Condition	Test ID	$p'_{pk}$ kPa	$q_{pk}$ kPa	$e_{pk}$
Type 1	Original	Tx_T1_4	229	389	0.89
		Tx_T1_5	414	634	0.87
	Evolved	Tx_T1_12	217	349	0.82
		Tx_T1_13	448	740	0.77
		Tx_T1_14	868	1392	0.77
Type 2	Evolved	Tx_T2_9	465	782	0.72
Type 3	Evolved	Tx_T3_12	194	278	1.08
		Tx_T3_13	204	305	1.06
		Tx_T3_14	205	317	1.01
		Tx_T3_15	375	522	1.09

**Table 5.** Critical state parameters for the three tailings soil types.

Material	Condition	$\phi'_{cs}$ (°)	$M_c$ (-)	$\lambda_e$ (-)	$\Gamma$ (-)
Type 1	Original	35.0	1.42	0.053	1.24
	Evolved			0.056	1.17
Type 2	Original	34.5	1.40	0.037	1.04
	Evolved			0.051	1.06
Type 3	Original	33.6	1.36	0.054	1.43
	Evolved			0.050	1.35

Note that  $\lambda_e$  represents notation in natural logarithm.

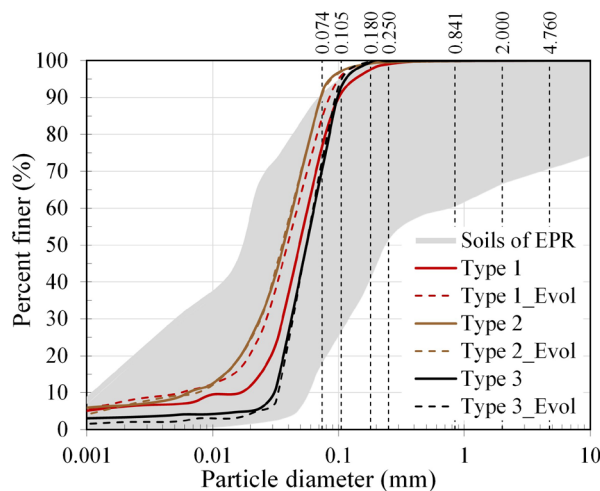


**Figure 12.** Grading curves of the three types of tailings in natural and evolved conditions. Comparison with other soils from Brumadinho dam, according to the Expert Panel Report (EPR) (Robertson et al., 2019).

the natural (original) state and another to the evolved state, as shown in Figure 11.

## 5.2 Grading evolution

Given the observed changes in soil behaviour, in terms of the critical state parameters, from tests in natural (remoulded) and evolved (reused soil after testing), a series of particle size distribution analyses was performed to assess the effect of crushing (or particle breakage) and the consequent generation of fines, as a result of CSL tests. Figure 12 illustrates the grading evolution of the three types of tailings.

From these results, the evolution of the behaviour in the Type 1 tailing can be attributed to the breakage of particles, which increased the fines content of the sample and consequently the compressibility of this material. However, no significant crushing was observed in Type 2 and Type 3 tailings. Changes in the morphology of the particles can also trigger the evolution of the behaviour of the material (Cho et al., 2006; Yang & Luo, 2015).

## 5.3 Morphological evolution

The assessment of the changes in particle morphology can be made by the careful observation of microscopic images of the soil in natural (intact) and evolved (after testing) conditions and by the identification of morphology parameters, such as sphericity, convexity, roughness and aspect ratio. For this purpose, scanning electron microscopy (SEM) photographs of the three types of tailings, in natural and evolved conditions, were taken and compared to observe changes in the morphology of the particles. As an example, SEM photos of natural and evolved samples of Types 1 and 3 are shown in Figure 13.

Due to the subjective nature of the visual description, the particle shape of a given soil should be described in quantitative terms such as morphology parameters, and a robust laser scanning technique must be used to make objective and accurate measurements of particle shape. This topic will be addressed in future works.

## 6. Characterisation in diverse stress-path conditions

### 6.1 Specific equipment and procedures

Flow liquefaction is a process associated with a pore pressure increase, by which shear strength is reduced as effective stress in the soil approaches zero and is intrinsically related to undrained brittle behaviour of the soil. Only contractive materials have the possibility of undergoing liquefaction. Since the failure of dam B1 involved the phenomenon of flow liquefaction, a proper consideration of the undrained behaviour of the tailing should rely on tests that adopt an initial stress state representative of the in-situ conditions ( $K_0$ ) and specific stress loading paths occurring in the geotechnical structures. For this purpose, a set of anisotropically consolidated undrained tests were carried out on loose (and even dense samples) to portray the liquefaction, strain softening and strain hardening behaviour of the three tailings. Table 6 summarises the adopted testing program for the undrained behaviour characterisation for the three types of tailings. The correct characterisation of the undrained peak strength is of utmost importance in the

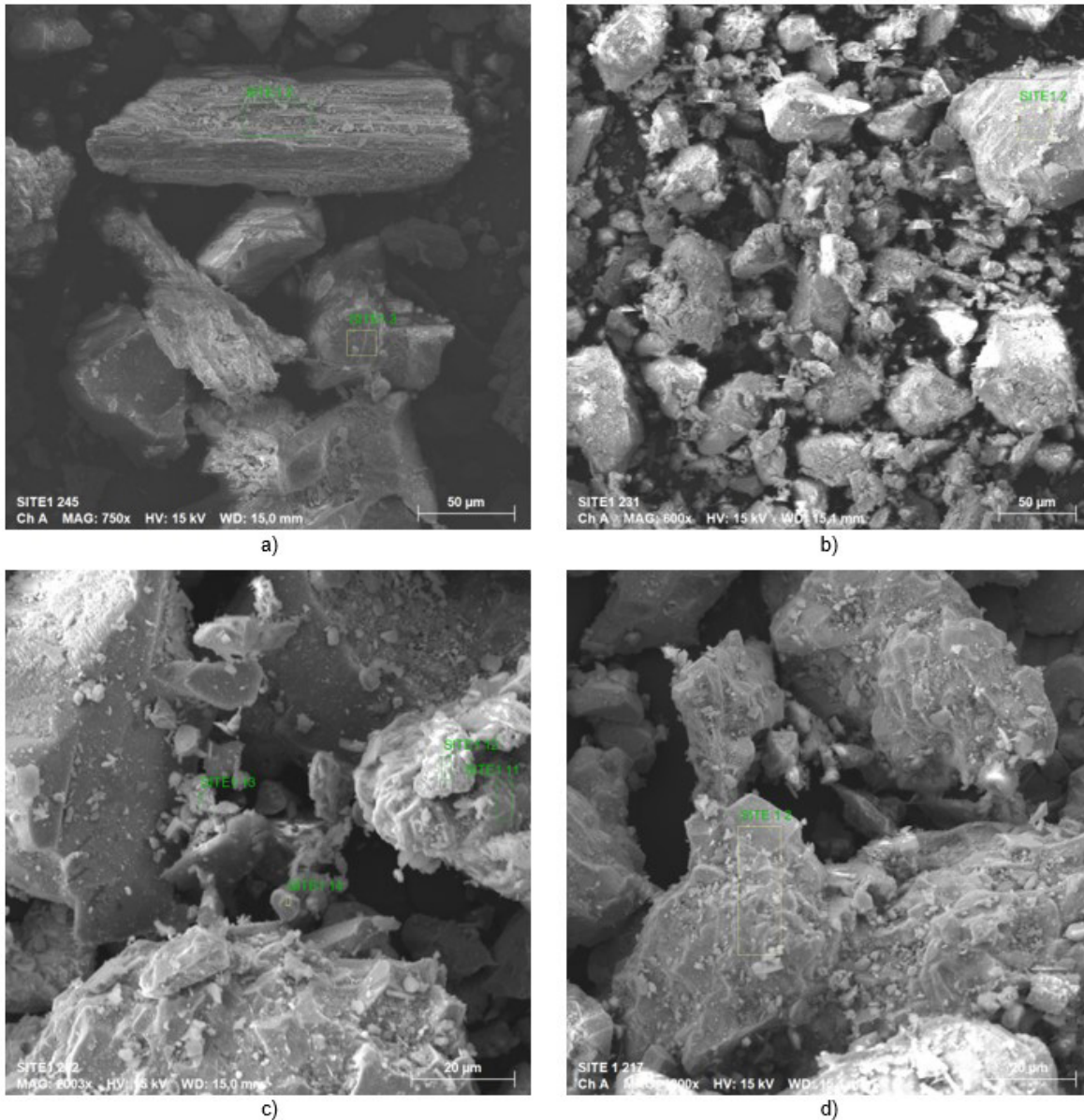


**Figure 13.** SEM images: Type 1 (a) natural; (b) evolved; Type 3 (c) natural; (d) evolved.

context of stability computations, as it signals the onset of instability (the inability of a soil specimen to sustain a given load or stress).

A fully automated Bishop-Wesley type triaxial apparatus, able to test soil specimens with 50 mm diameter, was used to carry out tests at different stress-path conditions. This triaxial apparatus can independently apply radial and axial stresses under strain or stress control, allowing the soil characterisation under any stress-path combination, representative of the complex behaviour of tailings dams. Besides, it was equipped with piezoelectric transducers for measuring seismic wave velocities (namely P-wave and S-wave) by bender element testing.

The specimens were prepared under very loose conditions (to replicate the deposition process in the tailing dam over the years of operation) using the same techniques previously described. A full saturation condition with  $B$ -values higher than 0.98 was achieved applying the same procedures as in the tests performed to reach ultimate critical state. The importance of full saturation is even more pronounced in undrained tests since the development of pore-water pressure strongly depends on the stiffness of the pore fluid. The samples were anisotropically consolidated at different mean effective stresses with a coefficient of lateral earth pressure at rest ( $K_0$ ) of approximately 0.5. Different undrained shear rates, including strain and stress control, were adopted to assess the effects of loading conditions on the behaviour

**Table 6.** Summary of the undrained testing program for the three tailings soil types.

Soil		Test ID	Test Type	Preparation State	Consolidation Phase		Shear Phase	
Type	Condition				$K_0$	$p'$ (kPa)	Type	Rate
Type 1	Original	SP_T1_1	CK <sub>0</sub> U	Loose	0.5	100	Stress Control (q)	1 kPa/min
		SP_T1_2	CK <sub>0</sub> U	Loose	0.5	100	Stress Control (q)	1 kPa/min
		SP_T1_3	CK <sub>0</sub> U	Loose	0.4	200	Stress Control (q)	1 kPa/min
	Evolved	SP_T1_4	CK <sub>0</sub> U	Dense	0.5	500	Strain Control	0.02 mm/min
		SP_T1_5	CK <sub>0</sub> U	Loose	0.5	500	Strain Control	0.002 mm/min
		SP_T1_6	CK <sub>0</sub> U	Loose	0.5	500	Strain Control	0.2 mm/min
		SP_T1_7	CK <sub>0</sub> U	Loose	0.5	500	Strain Control	0.02 mm/min
Type 2	Original	SP_T2_1	CK <sub>0</sub> U	Loose	0.5	100	Stress Control (q)	1 kPa/min
		SP_T2_2	CK <sub>0</sub> U	Loose	0.5	300	Stress Control (q)	1 kPa/min
		SP_T2_3	CK <sub>0</sub> U	Loose	0.5	400	Strain Control	0.02 mm/min
	Evolved	SP_T2_4	CK <sub>0</sub> U	Loose	0.5	400	Strain Control	0.002 mm/min
		SP_T2_5	CK <sub>0</sub> U	Loose	0.5	400	Strain Control	0.2 mm/min
		SP_T2_6	CK <sub>0</sub> U	Dense	0.5	400	Strain Control	0.02 mm/min
Type 3	Original	SP_T3_1	CK <sub>0</sub> U	Loose	0.5	50	Stress Control (q)	1 kPa/min
		SP_T3_2	CK <sub>0</sub> U	Loose	0.5	100	Stress Control (q)	1 kPa/min
		SP_T3_3	CK <sub>0</sub> U	Loose	0.4	200	Stress Control (q)	1 kPa/min
		SP_T3_4	CK <sub>0</sub> U	Loose	0.5	100	Stress Control (q)	0.1 kPa/min
	Evolved	SP_T3_5	CK <sub>0</sub> U	Loose	0.5	100	Strain Control	0.2 mm/min
		SP_T3_6	CK <sub>0</sub> U	Loose	0.5	100	Strain Control	0.02 mm/min
		SP_T3_7	CK <sub>0</sub> U	Loose	0.5	100	Strain Control	0.002 mm/min
		SP_T3_8	CK <sub>0</sub> U	Dense	0.5	100	Strain Control	0.02 mm/min

Legend: CK<sub>0</sub>U – anisotropic consolidated undrained tests.

of the studied soils, as referred in Table 6. The estimation of the final void ratio of soil specimens was carried out by measuring the water content after testing, however EOTSF was not used in the tests conducted in the Bishop-Wesley triaxial apparatus because of the handling of these heavy cells and to avoid damage to the BE. For these tests, the specimens were carefully removed from the cell, avoiding possible loss of soil particles and water (Verdugo & Ishihara, 1996), which –if used correctly– may be equally accurate to the EOTSF (Viana da Fonseca et al., 2021). A database containing the results of this advanced experimental program is also available in the form of Supplementary data to this paper.

## 6.2 Undrained anisotropic behaviour

The stress and state paths of the test performed to assess the undrained behaviour are presented in Figure 14.

In this testing program, all loose samples exhibit positive pore water pressure, revealing the tendency to contractive response over a wide range of confining pressures, as for the dense samples, a stable behaviour was observed. Some of the loose samples presented full liquefaction, with the

annulment of the mean effective stress and deviator stress, while others suffered severe strain softening but with not full liquefaction (i.e., zero effective stress), as a stable critical state is reached. In practice, both instability mechanisms would lead to catastrophic results. The undrained tests featured on Figure 14 highlighted the undrained brittleness in the tailings.

The peak strength points for those samples who experienced instability mechanisms allowed the definition of the instability line (IL) in the  $q - p'$  plane. The stress ratio ( $\eta_{pk} = \frac{q_{pk}}{p'_{pk}}$ ) at which peak is reached is about 0.93, 0.94 and 0.89 for the tailing type 1, 2 and 3, respectively. The uniqueness of the instability line in the stress invariant plane is assumed for each soil, and while these criteria have proven useful for limit equilibrium calculations, it is difficult to implement as calibration constraints in the context of numerical modelling (Mánica et al., 2021). From an implementation standpoint, the normalised undrained strength ratio  $S_p = \frac{S_{u, pk}}{p'_0}$  is preferred.

It offers a good template description of undrained peak strength in materials exhibiting static liquefaction and is the

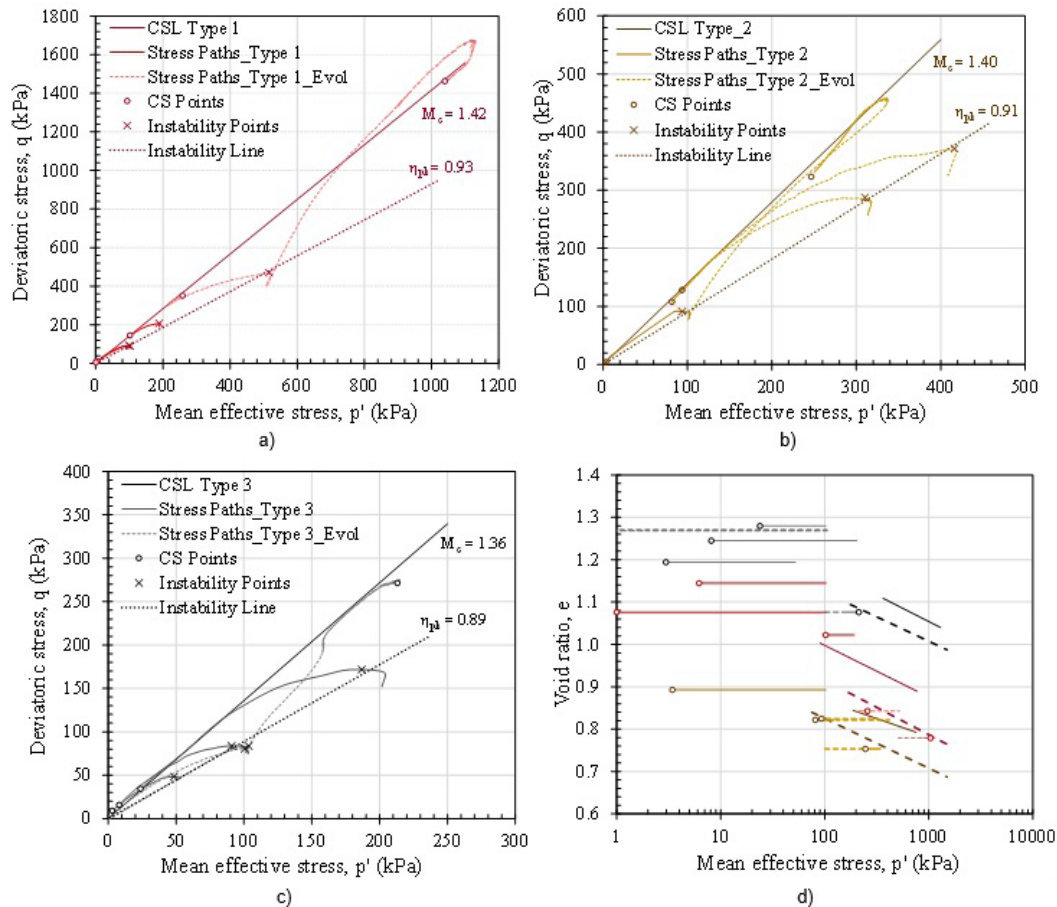


Figure 14. Undrained paths on the  $q - p'$  and  $e - \log p'$  plane for the different type of tailings.

reason between the peak undrained strength ( $s_{u,pk} = \frac{q_{pk}}{2}$ ) and the mean effective stress after soil consolidation ( $p'_d$ ).

Figure 15 shows the relationships between the undrained peak strength and the consolidation mean effective stress derived from the undrained triaxial compression tests that exhibit instability mechanisms. The undrained isotropic consolidated tests presented in the CSL section were also added for comparison. The interesting aspect is that the normalised undrained strength ratio did not depend on the type and condition of the soil but on the consolidation path, presenting much larger values of  $S_p$  for anisotropic consolidation than for isotropic. The underlying reason is that soil fabric is strain-path dependent (Fourie & Tshabalala, 2005).  $S_p$  is dependent on the fabric associated with anisotropy and particle orientation.

The figure clearly shows that the undrained peak strength ratio towards mean effective stress  $[(q/p'_p)]$  when starting from isotropic consolidation stresses ( $K = \sigma'_{ht}/\sigma'_{vt} = 1$ ) is considerably lower, about half, that at anisotropic consolidation stresses ( $K_0 = \sigma'_{ho}/\sigma'_{vo}$ , in this case assumed equal to 0.5). Thus, the at rest consolidation condition, assumed representative, should be considered for the modelling of TSF since the maximum undrained strength, which indicates the onset of soil instability,

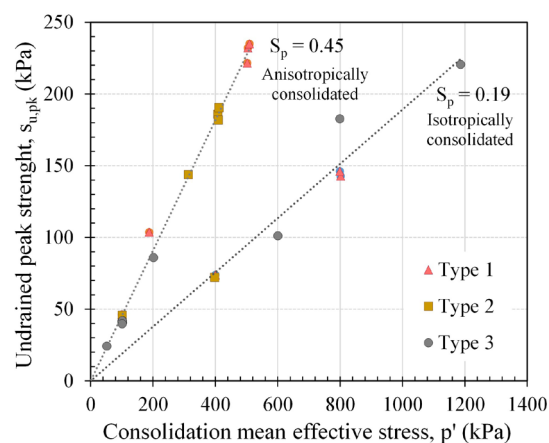
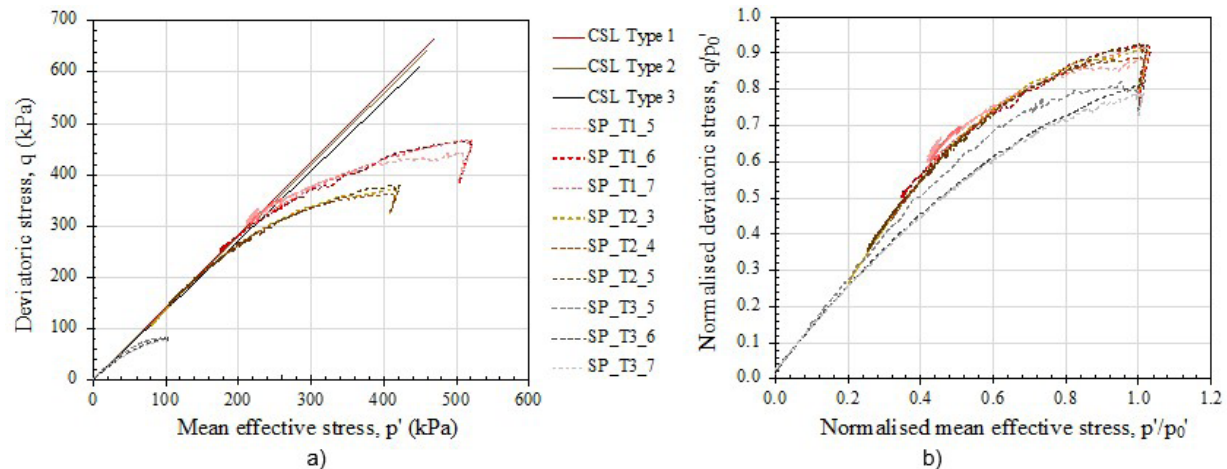


Figure 15. Relation between peak undrained strength and pre-shear consolidation stresses.

depends on the in-situ coefficient of earth pressure at rest (among other factors like stress rotation - see Reid et al., 2022). This also demonstrates the distinct effect of induced stress-anisotropic consolidation conditions on soil behaviour, which has design implications both in limit equilibrium calculations, especially when conducted in effective stresses analyses





**Figure 16.** Assessment of stress-strain dependency on the different tailing types.

(Fourie and Tshabalala, 2005), and in the assessment of soil state. In modelling the behaviour of these fragile soils, the resulting undrained peak strength will depend on the specific path by which the failure criterion is attained (Mánica et al., 2021). Studies are progressing for clarification of these factors.

### 6.3 Assessment of creep or stress-strain dependency

To evaluate creep behaviour, strain rate effects on the tailings were systematically measured in the different reconstituted materials using strain-rate controlled triaxial tests. For this effect, three triaxial specimens of each material under the same consolidation state (density and confining pressure) were sheared, in which the undrained strain rate was systematically varied in a magnitude order of 10%. This set of tests is identified in Table 6 as SP\_T1\_5, SP\_T1\_6 and SP\_T1\_7 for Type 1; SP\_T2\_3, SP\_T2\_4 and SP\_T2\_5 for Type 2; and SP\_T3\_5, SP\_T3\_6 and SP\_T3\_7 for Type 3.

The tests results are presented in Figure 16. The observed effect is equivalent to a change in undrained strength of 2% per order of magnitude change in strain rate. This experimental result suggests that the magnitude of measured strain-rate effects on the tailings was always small and did not anticipate a large role for viscous effects (or “creep”) in the failure.

The experimental result shown in Figure 16 suggests that the magnitude of measured strain-rate effects on the tailings was always small and did not anticipate a large role for viscous effects (or “creep”) in failure.

## 7. Conclusions

This paper described the experimental forensic characterisation of Brumadinho B1 tailings dam, a case history, which suddenly failed on January 25<sup>th</sup> of 2019 in Minas Gerais (Brazil). This detailed characterisation comprised an advanced experimental programme using reconstituted samples of three representative soils from Brumadinho B1 tailings dam.

All tests presented herein were carried out in the Geotechnical Laboratory of the Civil Engineering department at the Faculty of Engineering of the University of Porto (Portugal). The results provided the physical, hydraulic, and mechanical parameters for conducting numerical simulations of the soil behaviour using constitutive models based on Critical State Soil Mechanics with Instability Locus.

The outcomes of the programme are summarised as follows.

- Representative typological classes of soils considered representative of the tailings stored in the dam were defined for this research. This selection included a quantitative procedure based on the analysis and comparison of particle size distribution and specific gravity of solid particles results, leading to three clusters with diverse iron and fines contents;
- An evolution of the mechanical behaviour of the studied tailings was observed in the three studied tailings. The evolution of the soil behaviour caused additional compressibility –represented by a shift down of CSL in the  $e - \log p'$  plane. However, it did not affect the friction angle of shearing resistance at the critical state. Such an evolution was attributed to changes in the morphology of soil particles and grain size distribution after triaxial testing, as evidenced in Figure 12 and 13;
- From the undrained tests, an instability line was inferred for each soil. However, a comparison between experimental results of isotropic and anisotropic tests revealed higher values of undrained shear strength for the soil specimens consolidated for  $K_0$  of about 0.5. This indicates that there is a significant effect of soil anisotropy on the undrained behaviour of iron tailings from the Brumadinho B1 dam;
- Tests conducted using a systematic combination of shear rates under strain and stress control revealed very similar shear-strain characteristics for all studied

soils. Therefore, negligible viscous effects or “creep” have been observed in the mechanical behaviour of these geomaterials.

## Acknowledgements

Acknowledgements are especially due to Prof. Marcos Arroyo and Prof. Antonio Gens, from CIMNE, who were directly involved in the definition of the lab tests to define the necessary constitutive parameters for the models used in the numerical analyses. This was done under a contract between CIMNE and VALE, SA, under a Term of Cooperation of the Federal Public Prosecutor’s Office, (MPF). FEUP, as partner of CIMNE, acknowledges VALE’s collaboration in the field and MPF support, namely in the sampling campaigns. For these, we owe a special and personal acknowledgement to Dr. Sebastião Oliveira (MPF) and Ing. Leonardo Mesquita (PF) for their commitment in organising, executing and illustrating the field work, which enabled the challenging work of collecting the representative samples and their transport to LabGEO in safe conditions, as attested by VALE, SA, officers. A friendly recognition to Prof. Antonio Mendonça of the Federal University of Minas Gerais (BH), for a precious and continuous dedication to sampling and conditioning works, especially in the 2<sup>nd</sup> and 3<sup>rd</sup> campaigns. The experimental work in FEUP and the interpretation of the results was financially supported by the referred contract between CIMNE and VALE, and, as agreed with MPF, was also part of the research activities of CONSTRUCT– Institute of Research and Development (R&D) in Structures and Construction, funded by national funds through the FCT/MCTES (PIDDAC), with the Base Funding –UIDB/04708/2020.

## Declaration of interest

Not applicable due to absence of conflicting interests.

## Authors’ contributions

António Viana da Fonseca: Conceptualisation, Methodology, Validation, Investigation, Resources, Data Curation, Writing - Original Draft & Review, Supervision, Project administration and Funding acquisition. Diana Cordeiro: Conceptualisation, Methodology, Formal analysis, Investigation, Data Curation, Writing - Review & Editing, Visualisation. Fausto Molina-Gómez: Conceptualisation, Formal analysis, Investigation, Visualisation, Writing – review & editing. Davide Besenon: Formal analysis, Investigation, Data Curation, Writing – review & editing. António Fonseca: Methodology, Investigation, Data Curation, Writing, Visualisation. Cristiana Ferreira: Formal analysis, Visualisation, Writing – review & editing.

## List of symbols

$e$	void ratio
$e_0$	initial void ratio
$e_{cs}$	critical state void ratio
$e_{pk}$	void ratio at the peak value of maximum dilation
$k$	coefficient of hydraulic conductivity
$p'_0$	mean effective stress of consolidation
$p'_{pk}$	mean effective stress at the peak value of maximum dilation
$q$	deviatoric stress
$q_{pk}$	peak deviatoric stress
$s_{u, pk}$	peak undrained shear strength
<i>ASTM</i>	American Society for Testing and Materials
$B$	Skempton’s pore pressure coefficient
<i>BE</i>	Bender Elements
$Bq$	pore-pressure index
$Cc$	compressibility index
<i>CIAEA</i>	Extraordinary Independent Consulting Committee for Investigation
<i>CIMNE</i>	International Centre for Numerical Methods in Engineering
<i>CID</i>	Isotropic consolidated drained tests
<i>CIU</i>	Isotropic consolidated undrained tests
$CK_0U$	Anisotropic consolidated undrained tests
$CO_2$	Carbon Dioxide
<i>CPTu</i>	Piezcone Penetration Test
$Cr$	Recompressibility index
$Cs$	Expansion index
<i>CSL</i>	Critical State Locus
<i>CSSM</i>	Critical State Soil Mechanics
$C_u$	coefficient of uniformity
<i>EOTSF</i>	End-of-test soil freezing
<i>EPR</i>	Expert Panel Technical Report
<i>FC</i>	Fines Content
<i>FEUP</i>	Faculty of Engineering of the University of Porto
$G_s$	Specific gravity of solid particles
$I_c$	Soil behaviour type index
<i>ID</i>	Identification
<i>IL</i>	Instability Locus
<i>ISO</i>	International Organisation for Standardisation
$K_0$	Coefficient of earth pressure at rest
<i>LabGEO</i>	Geotechnical Laboratory of the Civil Engineering Department at FEUP
<i>LiDAR</i>	Laser imaging, Detection, and Ranging
$M_c$	Slope of critical state locus in $q-p'$ plane in compression
<i>MG</i>	Minas Gerais
<i>MPF</i>	Federal Public Prosecutor’s Office
$N$	Intercept of normal compression line in $e-\log p'$ plane
$p'$	Mean effective stress
<i>PSD</i>	Particle Size Distribution
<i>SBT</i>	Soil Behaviour Type
<i>SDMT</i>	Seismic Flat Dilatometer Test
<i>SEM</i>	Scanning Electron Microscopy

$S_p$	Normalised undrained strength ratio
$T_{SF}$	Tailings Storage Facility
$UFMG$	Federal University of Minas Gerais
$U_n$	Percent of undercompaction
$UPC$	Universitat Politècnica de Catalunya
$V_p$	P-wave velocity
$V_s$	S-wave velocity
$\phi'_{cs}$	Friction angle at the critical state
$\phi'_{pk}$	Peak friction angle
$\kappa$	Slope of unloading–reloading line in $e$ -log $p'$ plane
$\lambda_e$	Slope of normal compression line / slope of critical state line in $e$ -log $p'$ plane
$\eta_{pk}$	Stress ratio at peak undrained strength
$\sigma'_v$	Vertical effective stress
$\psi$	State parameter
$\Gamma$	Intercept of critical state line in $e$ -log $p'$ plane

## References

- Bedin, J., Schnaid, F., Viana da Fonseca, A., & de Costa Filho, L.M. (2012). Gold tailings liquefaction under critical state soil mechanics. *Geotechnique*, 62(3), 263-267. <http://dx.doi.org/10.1680/geot.10.P.037>.
- Been, K., & Jefferies, M. (2011). Stress-dilatancy in very loose sand. *Canadian Geotechnical Journal*, 41(5), 972-989. <http://dx.doi.org/10.1139/T04-038>.
- Cho, G.-C., Dodds, J., & Santamarina, J.C. (2006). Particle shape effects on packing density, stiffness, and strength: natural and crushed sands. *Journal of Geotechnical and Geoenvironmental Engineering*, 132(5), 591-602. [http://dx.doi.org/10.1061/\(ASCE\)1090-0241\(2006\)132:5\(591\)](http://dx.doi.org/10.1061/(ASCE)1090-0241(2006)132:5(591)).
- CIMNE (2021). *Computational analyses of Dam I failure at the Corrego de Feijao mine in Brumadinho – Final Report*. Retrieved in February 4, 2022, from <http://www.mpf.mp.br/mg/sala-de-imprensa/docs/2021/relatorio-final-cinme-upc-1>
- Ferreira, C., Díaz-Durán, F., Viana da Fonseca, A., & Cascante, G. (2021). New approach to concurrent VS and VP measurements using bender elements. *Geotechnical Testing Journal*, 44(6), 1801. <http://dx.doi.org/10.1520/GTJ20200207>.
- Fourie, A.B., & Tshabalala, L., (2005). Initiation of static liquefaction and the role of K0 consolidation. *Canadian Geotechnical Journal*, 42(3), 892-906. <https://doi.org/10.1139/t05-026>.
- ISO 17892-3. (2015). *Geotechnical investigation and testing – Laboratory testing of soil – Part 3: Determination of particle density*. International Organisation for Standardisation.
- ISO 17892-4. (2016). *Geotechnical investigation and testing – Laboratory testing of soil – Part 4: Determination of particle size distribution*. International Organisation for Standardisation.
- ISO 17892-5. (2017). *Geotechnical investigation and testing – Laboratory testing of soil – Part 5: Incremental loading oedometer test*. International Organisation for Standardisation.
- ISO 17892-9. (2018). *Geotechnical investigation and testing – Laboratory testing of soil – Part 9: Consolidated triaxial compression tests on water saturated soils*. International Organisation for Standardisation.
- Jefferies, M., & Been, K. (2016). *Soil liquefaction: a critical state approach* (2nd ed.). CRC Press.
- Ladd, R. (1978). Preparing test specimens using undercompaction. *Geotechnical Testing Journal*, 1(1), 23. <http://dx.doi.org/10.1520/GTJ10364J>.
- Mánica, M.A., Arroyo, M., Gens, A., & Monforte, L. (2021). Application of a critical state model to the Merriespruit tailings dam failure. *Proceedings of the Institution of Civil Engineers – Geotechnical Engineering*. [ahead of print]. <https://dx.doi.org/10.1680/JGEEN.21.00001>.
- Molina-Gómez, F., & Viana da Fonseca, A. (2021). Key geomechanical properties of the historically liquefiable TP-Lisbon sand. *Soil and Foundation*, 61(3), 836-856. <http://dx.doi.org/10.1016/J.SANDF.2021.03.004>.
- Reid, D., Dickinson, S., Mital, U., Fanni, R., & Fourie, A. (2022). On some uncertainties related to static liquefaction triggering assessments. *Proceedings of the Institution of Civil Engineers – Geotechnical Engineering*. [ahead of print]. <https://doi.org/10.1680/jgeen.21.00054>.
- Reid, D., Fourie, A., Ayala, J.L., Dickinson, S., Ochoa-Cornejo, F., Fanni, R., Garfias, J., Viana da Fonseca, A., Ghafghazi, M., Ovalle, C., Riemer, M., Rismanchian, A., Olivera, R., & Suazo, G. (2021). Results of a critical state line testing round robin programme. *Geotechnique*, 71(7), 616-630. <http://dx.doi.org/10.1680/JGEOT.19.P.373>.
- Robertson, P.K., & Wride, C.E. (1998). Evaluating cyclic liquefaction potential using the cone penetration test. *Canadian Geotechnical Journal*, 35(3), 442-459. <http://dx.doi.org/10.1139/t98-017>.
- Robertson, P.K., de Melo, L., Williams, D.J., & Wilson, G.W. (2019). *Report of the expert panel on the technical causes of the failure of Feijão Dam I*. Retrieved in February 4, 2022, from <http://www.b1technicalinvestigation.com/>
- Santamarina, J.C., Klein, K.A., & Fam, M.A. (2001). *Soils and waves*. J. Wiley & Sons.
- Smith, K., Fanni, R., Chapman, P., & Reid, D. (2019). Critical state testing of tailings: comparison between various tailings and implications for design. In *Proceedings of Tailings and Mine Waste* (pp. 1183-1195). Vancouver.
- Soares, M., & Viana da Fonseca, A. (2016). Factors affecting steady state locus in triaxial tests. *Geotechnical Testing Journal*, 39, 1056-1078. <http://dx.doi.org/10.1520/GTJ20150228>.
- Verdugo, R., & Ishihara, K. (1996). The steady state of sandy soils. *Soil and Foundation*, 36(2), 81-91. [http://dx.doi.org/10.3208/sandf.36.2\\_81](http://dx.doi.org/10.3208/sandf.36.2_81).
- Viana da Fonseca, A., Cordeiro, D., & Molina-Gómez, F. (2021). Recommended procedures to assess critical state locus from triaxial tests in cohesionless remoulded

samples. *Geotechnics*, 1, 95-127. <http://dx.doi.org/10.3390/GEOTECHNICS1010006>.

Viana da Fonseca, A., Ferreira, C., & Fahey, M. (2009). A framework interpreting bender element tests, combining time-domain and frequency-domain methods. *Geotechnical Testing Journal*, 32(2), 91-107. <http://dx.doi.org/10.1520/GTJ100974>.

Yang, J., & Luo, X.D. (2015). Exploring the relationship between critical state and particle shape for granular

materials. *Journal of the Mechanics and Physics of Solids*, 84, 196-213. <https://doi.org/10.1016/J.JMPS.2015.08.001>.

### Supplementary data

All data reported in this paper is fully available as supplemental material at the following locations: <https://s.up.pt/jvo1> and <https://s.up.pt/m13m>